Modeling and Identification of a Nonlinear SDOF Moored Structure, Part 2—Comparisons and Sensitivity Study

S.C.S. Yim
Department of Civil Engineering,
Oregon State University,
Corvallis, OR 97331 USA
e-mail: solomon.yim@oregonstate.edu

S. Narayanan
Skillings-Connolly, Inc.,
5016 Lacey Boulevard S.E.,
Lacey, WA 98503 USA
e-mail: chithra@skillings.com

A system-identification technique based on the Reverse Multiple-Input/Single-Output (R-MI/SO) procedure is applied to identify the parameters of an experimental mooring system exhibiting nonlinear behavior. In Part 1, two nonlinear small-body hydrodynamic Morison type formulations: (A) with a relative velocity (RV) model, and (B) with an independent-flow-field (IFF) model, are formulated. Their associated nonlinear system-identification algorithms based on the R-MI/SO system-identification technique: (A.1) nonlinear-structure linearly damped, and (A.2) nonlinear-structure coupled hydrodynamically damped for the RV model, and (B.1) nonlinear-structure nonlinearly damped for the IFF model, are developed for an experimental submerged-sphere nonlinear mooring system under ocean waves. The analytic models and the associated algorithms for parametric identification are described. In this companion paper (Part 2), we use the experimentally measured input wave and output system response data and apply the algorithms derived based on the multiple-input/single-output linear analysis of the reverse dynamic systems to identify the system parameters. The two nonlinear models are examined in detail and the most suitable physical representative model is selected for the mooring system considered. A sensitive analysis is conducted to investigate the coupled hydrodynamic forces modeled by the Morison equation, the nonlinear stiffness from mooring lines and the nonlinear response. The appropriateness of each model is discussed in detail. [DOI: 10.1115/1.1710874]

Introduction

Two alternative small-body hydrodynamic Morison type models of coupled fluid-structure interaction excitations–(A) a relatively velocity (RV) model that fully couples wave motion and dynamic structural response, and (B) an independent flow-field (IFF) model that decouples the fluid and structural velocities, have been formulated in Part 1 [1]. For the RV model, a straightforward system identification algorithm (A.1)—nonlinear-structure linearly damped (NSLD) is first derived using the reverse multi-input/single-output (R-MI/SO) technique. In addition, an iterative version (A.2) called nonlinear-structure coupled hydrodynamically damped (NSCHD) algorithm, has been derived to improve the accuracy of the identified parameters. For the IFF model, the associated algorithm (B.1) with a nonlinear-structure nonlinearly damped (NSND) assumption has been derived. In this paper (Part 2), the resulting systems using the identified parameters obtained based on these algorithms are employed to predict the responses of the fluid-structure interaction of the SDOF, symmetric spherical mooring system. A detailed study is conducted on the different reverse dynamic models to select the most physically representative model for the ocean mooring system considered is described herein.

The nonlinear multi-point moored submerged sphere experiment [2] conducted at the O. H. Hinsdale Wave Laboratory at Oregon State University (OSU) is employed in this study. The wave excitation input and the system responses measured during the test are used for parameter identification. Using the identified properties from each model, numerical predictions of the dynamic response are compared with the experimental results in both time and frequency domains to select the most suitable one for the system.

Using the measured wave excitation and response data together with the identified system parameters, a detailed study is performed on the response behavior of the system under consideration. A sensitivity analysis is conducted to determine the optimal range of system parameters and understand the effect of varying the stiffness and damping coefficients on the system response.

The RV and independent flow field (IFF) models require the knowledge of inertia and drag coefficients, C_m and C_d, respectively for the evaluation of hydrodynamic force. A vast library of experimental data on hydrodynamic coefficients for cylinders as a function of the Keulegan-Carpenter number (KC), the Reynolds number (Re) and the roughness parameters is available from laboratory and field tests. The real fluid effects, proximity of boundaries, fluid particle excursion lengths, surface roughness, vortex shedding, and non-harmonic motions tend to modify the forces on the cylinder thus yielding non-constant values for the hydrodynamic coefficients. Theoretical studies of unsteady motions involving a sphere in a real fluid have so far been restricted to small Reynolds numbers [3,4]. The C_m for fixed spheres was found to vary between 1.43 and 1.73 within the range of $0.2 \leqslant KC \leqslant 3.2$ [5]. For a pilot study in the ocean on wave-induced forces on a fixed sphere with the inertia forces dominating the total force and Re ranging from 10^5 to 5×10^5, Grace and Zee (1978) [6] found the average inertia coefficient to be 1.21 and the C_d to be 0.4. With the coefficients dependent on KC and Re, reasonable estimates of the hydrodynamic coefficients for a sphere are within the following bounds, $0.1 \leqslant C_d \leqslant 1.0$ and $1.0 \leqslant C_m \leqslant 1.5$ [6,7]. In this study, the R-MI/SO technique is also employed to evaluate the effects of hydrodynamic coefficients on system response by varying C_m and C_d within a range.

Contributed by the OOAE Division for publication in the JOURNAL OF OFFSHORE MECHANICS AND ARCTIC ENGINEERING. Manuscript received July 9, 2002; final revision, September 27, 2003. Associate Editor: B. Riggs.

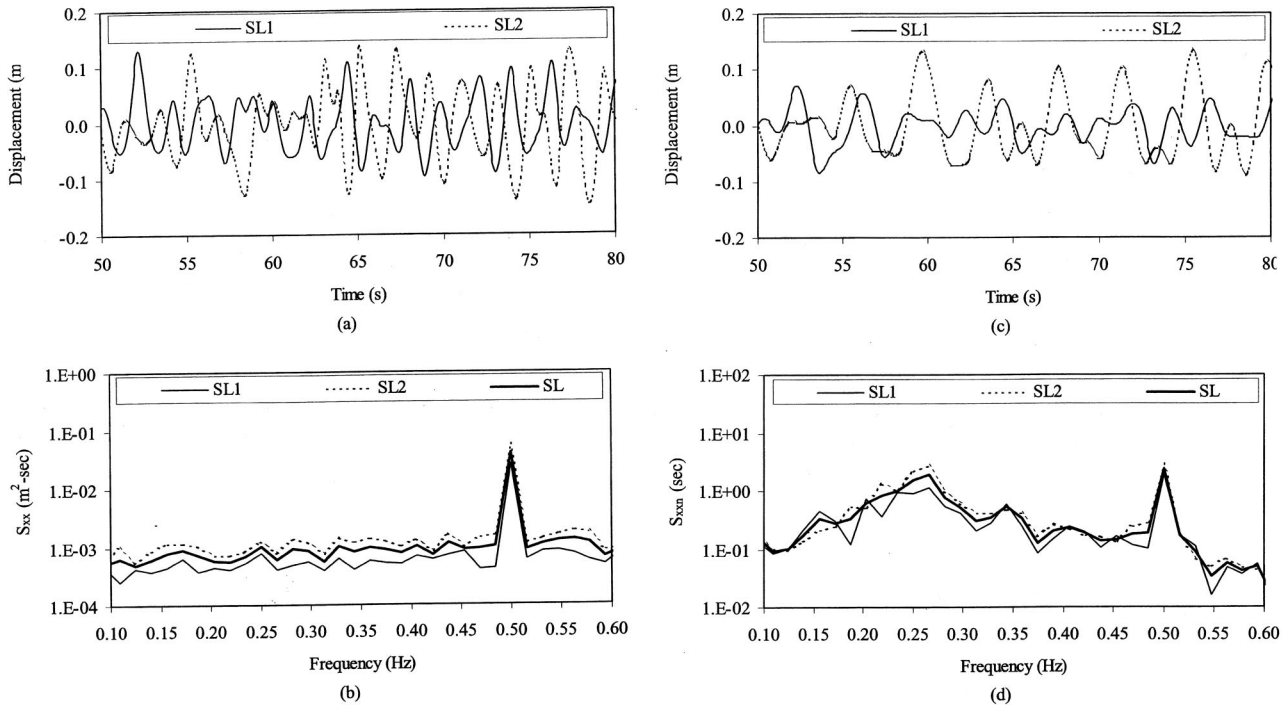

Fig. 1 SDOF experimental low wave amplitude data: *a*) wave time series, *b*) wave spectra, *c*) response time series, *d*) response spectra

Selection of Most Suitable Model

Two hydrodynamic models, resulting in three nonlinear system identification formulations discussed in Part 1 [1], have been applied to the experimental SDOF mooring system. Eight tests were conducted on the sphere with periodic plus white noise excitations [2]. The experimental data had been examined for accuracy and calibrated with independent measurements at the beginning and end of each day of tests. Drifts of the gages were not observed. Because the system is nonlinear, the means and trends have special significance and are not removed. All the experimental data have wave period of $T=2$ seconds with varying wave heights and noise/signal ratio. The wave displacement and surge response of the sphere were measured and the wave velocity and acceleration were numerically evaluated using a central-difference method [8]. Each of the tests displays a certain degree of subharmonics in the sphere movement. The data sets SL1, SL2, SM1, SM2, SM3, SH1, SH2 and SH3 are grouped according to wave excitation amplitudes, where S stands for single-degree-freedom, and L, M and H represents low, medium and high wave amplitudes, respectively. A typical segment of the wave time series and its corresponding spectra, and a typical segment of the response time series and its corresponding spectra for all the data sets grouped are given in Figs. 1–3. The mean spectra for the three groups, SL, SM and SH are also shown in the figures and are considered to be representative of each group. The input wave characteristics such as wave height (H), C_m, C_d, Keulegan Carpenter number (KC) and Reynolds number (Re) are shown in the Table 1.

The sampling interval used in the experiment was 0.0625 s (16 Hz), which yields a Nyquist frequency of 8 Hz. The total number of samples of the excitation and response time histories for spectral simulations is 8192 (512 s), with sub-record lengths of 1024 for the Fourier transforms (64 s).

The nonlinear system identification algorithms NSLD and NSCHD for the RV model, and NSND for the IFF model, are applied to all the data sets using the R-MI/SO technique presented in Part 1. The linear and nonlinear system parameters for the NSLD, NSCHD and NSND algorithms are determined using Eqs. (14d-e) and (21a-c), Eqs. (14d-e), (21a-c), and (23c), Eqs. (14d-e), (21a-c) and (25c), respectively, in Part 1. Using the identified parameters, the response is evaluated for each model by solving the respective ordinary differential equations, (Eqs. (12), (22) and (24) in Part 1) using a 4th-order Runge-Kutta method [8].

The predicted responses from the RV and IFF models are compared with the experimental response in the frequency domain for all the experimental data. The comparisons are shown for the three groups, SL, SM and SH in Fig. 4. It is observed that the primary resonance region for the two models peak at the same frequency as that for the experimental data with the RV and IFF models using NSCHD and NSND algorithm, respectively, have the energy level closer to that of the experimental data. These resonances correspond to the natural frequencies of the linear model, i.e., H(f). The RV model with the NSLD algorithm has a higher primary energy level. The subharmonic response simulated using RV model with NSLD and NSCHD algorithms does not compare well with the actual measured response. On the other hand, the response simulated for the IFF model using NSND algorithm matches well with the experimental response both in the primary as well as the subharmonic resonance regions. As discussed in the Hydrodynamic Force Models Section in Part 1, for low KC and high V_R (reduced velocity), as in the case of the experimental system considered, the RV model may not be appropriate [9]. Due to the lack of a comprehensive experimental study on the determination of the appropriate forms of the Morison equation (which itself is empirical) for different combinations of parameters and experimental settings, it has been difficult to assess the appropriateness of the various forms of the Morison hydrodynamic force expression. But in this study, using the R-MISO technique, linear and nonlinear system parameters for different models are determined and a response is simulated, that is compared with the experimental response to evaluate the appropriateness of different forms of force models. Hence, the IFF model using the NSND algorithm represents the experimental system very well. A comparison of time series and spectra between the identified response using the IFF model and the experimental response is shown in

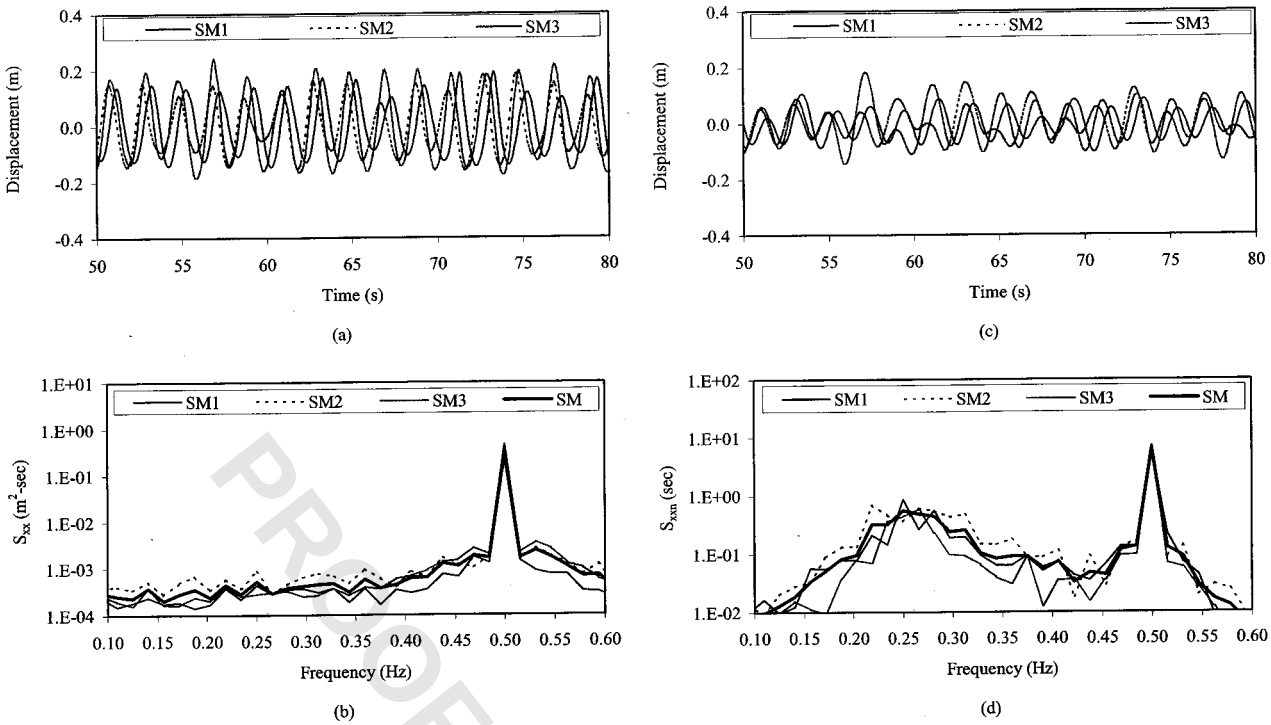

Fig. 2 SDOF experimental medium wave amplitude data: *a*) wave time series, *b*) wave spectra, *c*) response time series, *d*) response spectra

Fig. 5. The system parameters, a_1, a_2, a_3, ζ_1 and C'_{d1} identified for all the test data using the IFF model are given in Table 2.

Sensitivity Analysis

A parametric study is performed to determine the sensitivity of the system to variations in the parameters. Specifically, each parameter is varied in prescribed increments while keeping all other identified parameters constant (Table 2) and the surge response is computed for each variation by solving (Eq. (24), Part 1). The simulated responses using the identified parameters are compared against each other in both the time and frequency domains.

From the parametric study, an optimal range and the most suit-

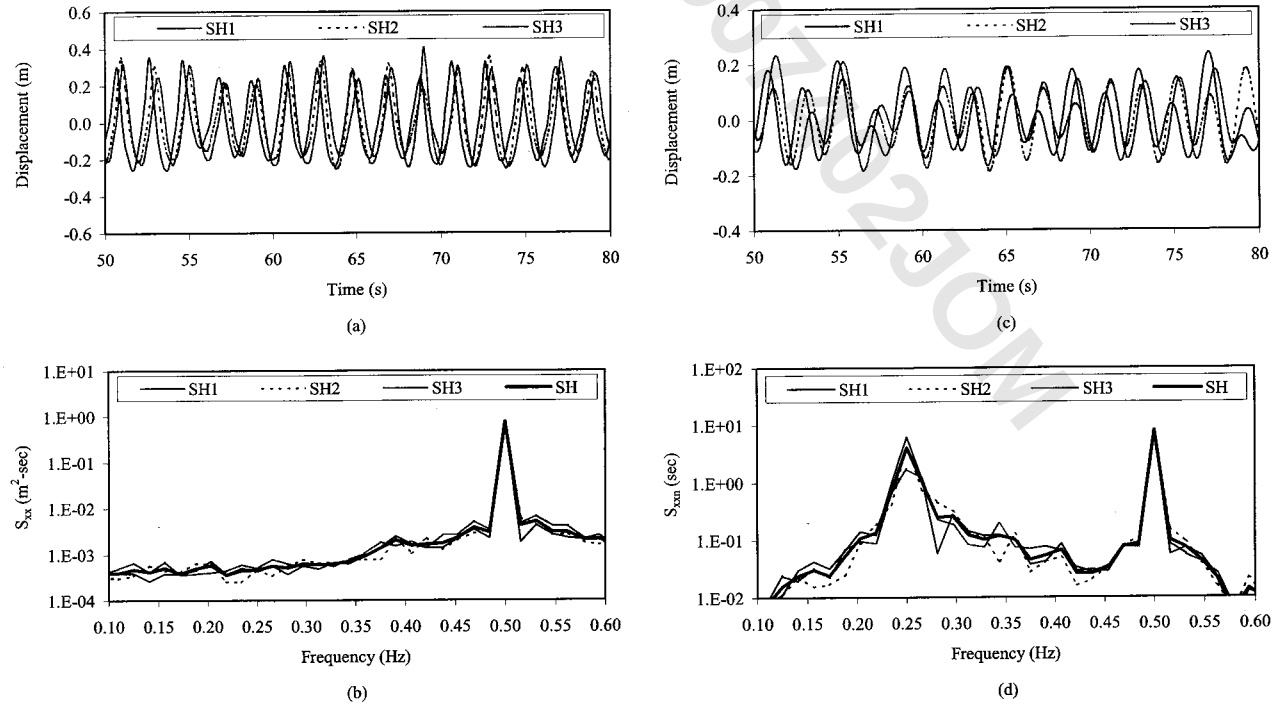

Fig. 3 SDOF experimental high wave amplitude data: *a*) wave time series, *b*) wave spectra, *c*) response time series, *d*) response spectra

Table 1 Input wave characteristics of the SDOF subharmonic data

Data	H (m)	C_m	C_d	KC_F	Re_F
SL1	0.17	1.4	0.1–0.9 (0.5)	0.56	5.70E4
SL2	0.24	1.4	0.1–0.9 (0.5)	0.79	7.80E4
SM1	0.35	1.3	0.1–0.9 (0.5)	1.18	1.20E5
SM2	0.36	1.3	0.1–0.9 (0.5)	1.18	1.20E5
SM3	0.49	1.3	0.1–0.9 (0.5)	1.57	1.60E5
SH1	0.66	1.1	0.1–0.9 (0.5)	2.16	2.20E5
SH2	0.66	1.1	0.1–0.9 (0.5)	2.18	2.22E5
SH3	0.67	1.1	0.1–0.9 (0.5)	2.20	2.30E5

able value of the system parameters are obtained and tabulated in Table 3. Because the data sets belong to L, M, and H groups exhibit similar behavior; only the mean of the resulting spectra for each variation is discussed in the following paragraphs.

The effect of varying linear stiffness coefficient, a_1 on SL, SM and SH are demonstrated in Fig. 6. The spectral density normalized with the variance of experimental wave data (S_{xxn}) is plotted against frequency for a_1 from 58.0 to 202.9 N/m or a1n (the ratio of instantaneous value of a_1 to the best value of a_1 as given in Table 4) from 0.5 to 1.6. It can be observed that there is a slight increase in the primary resonance response as a_1 increases. The subharmonic resonance region shifts towards the right with increasing a_1. The trend can be observed more clearly (from SL to SH) as the wave amplitude increases.

When a_2 is increased from 0 to 476.6 N/m^2, there is no significant change in the data group SL as shown in Fig. 7*a*. However, the response in the secondary resonance region increases from a2n=0 to 2.5 for SM and SH, and the effects are more pronounced for the latter (Fig. 7*b* and 7*c*). The total energy of the response in the primary resonance region is affected by changing a_2.

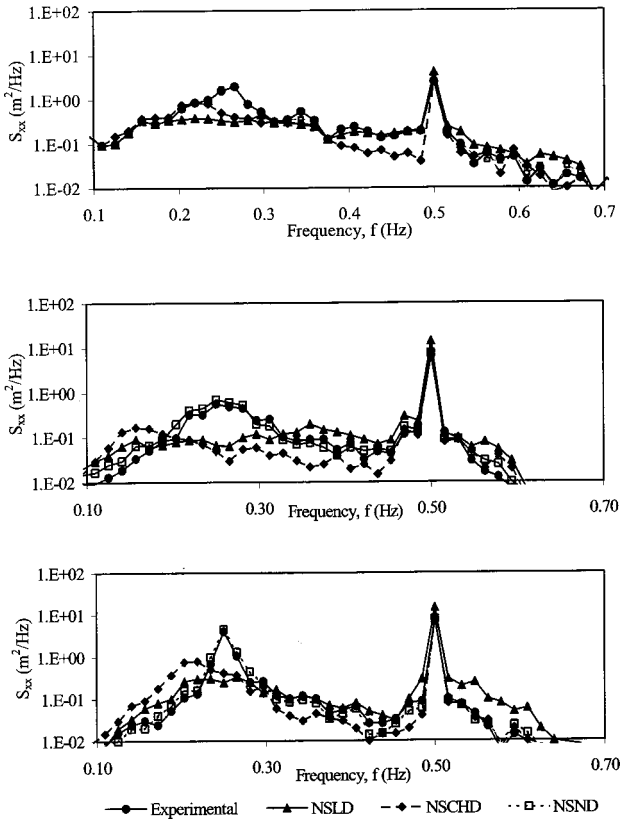

Fig. 4 Comparison of identified responses using alternative algorithms with the experimental response *a*) SL *b*) SM *c*) SH

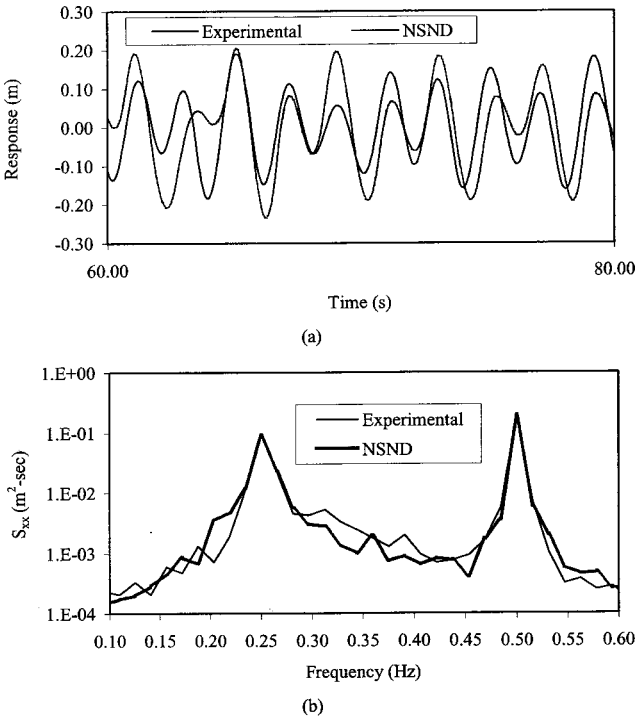

Fig. 5 Comparison of simulated response using IFF model with the experimental response: *a*) time series, *b*) spectra (Note: Captions will be modified–"NSND" will be changed to "IFF")

Figure 8 shows that varying a_3 from 0 to 1568.1 N/m^3 or a3n from 0 to 2.5 affects only the response in the secondary resonance region, which decreases as a_3 increases. The variation is most noticeable for SH in Fig. 8*c*.

With regards to varying the linear structural damping coefficient ζ_1 from 0 to 0.1, it is observed that the response in the subharmonic region decreases with increasing damping while the primary resonance region remains unaffected as demonstrated in Fig. 9. This result indicates that the subharmonic response is sensitive to structural damping. This phenomenon is often observed in responses of nonlinear systems.

The effects of varying C'_{d1} on the identified response are demonstrated in Fig. 10. It shows that the secondary resonance region generally decreases with increasing C'_{d1}. However, the optimum range that identify response comparable to the experimental response differs for the data groups SL, SM and SH. The most suitable value goes as high as 2 for SL and it decreases to 0.5 for SM and 0.15 for SH. This apparent behavior is probably caused by the inability of the model to approximate accurately the actual

Table 2 Identified system parameters of the SDOF subharmonic data

Data	a_1 (N/m)	a_2 (N/m^2)	a_3 (N/m^3)	C'_{d1}	ζ_1 (%)	f_{n1} (Hz)
SL1	128.8	315.6	721.3	2.5	3.5	0.22
SL2	125.6	280.1	814.7	3.5	3.4	0.23
SM1	128.8	260.8	863.0	3.0	3.0	0.23
SM2	132.0	257.6	769.6	1.5	2.9	0.24
SM3	125.6	206.1	689.1	1.0	2.8	0.23
SH1	128.8	209.3	689.1	0.8	3.0	0.23
SH2	128.8	209.3	689.1	0.2	3.2	0.23
SH3	125.6	190.0	627.9	0.3	3.1	0.22

Table 3 Identified system parameters from the sensitivity analysis of the SDOF subharmonic data

Data	a_1 (N/m)	a_2 (N/m^2)	a_3 (N/m^3)	C'_{d1}	ζ_1 (%)	f_{n1} (Hz)
SL1	122.4–32.0 (128.8)	48.3–378.0 (215.7)	157.8–1410.4 (772.8)	1.5–2.5 (2.0)	1.0–4.0 (3.0)	0.23
SL2	119.1–132.0 (125.6)	48.3–380.0 (215.7)	157.8–1410.4 (772.8)	1.5–2.5 (2.0)	1.0–4.0 (3.0)	0.23
SM1	122.4–132.0 (128.8)	48.3–380.0 (215.7)	157.8–1255.8 (708.4)	1.5–2.5 (2.0)	1.5–4.0 (3.3)	0.23
SM2	122.4–135.2 (128.8)	141.7–286.6 (215.7)	470.1–933.8 (708.4)	0.3–0.7 (0.5)	2.0–4.0 (3.0)	0.24
SM3	122.4–135.2 (125.6)	141.7–286.6 (215.7)	470.1–933.8 (708.4)	0.3–0.7 (0.5)	2.0–4.0 (3.0)	0.23
SH1	122.4–138.5 (132.0)	167.4–286.6 (225.4)	550.6–933.8 (740.6)	0.1–0.2 (0.15)	2.5–4.0 (3.3)	0.23
SH2	122.4–135.2 (128.8)	190.0–238.3 (215.7)	627.9–772.8 (708.4)	0.1–0.2 (0.15)	2.0–4.0 (3.0)	0.23
SH3	122.4–135.2 (132.0)	199.6–238.3 (219.0)	660.1–772.8 (708.4)	0.1–0.2 (0.15)	2.0–4.0 (3.0)	0.22

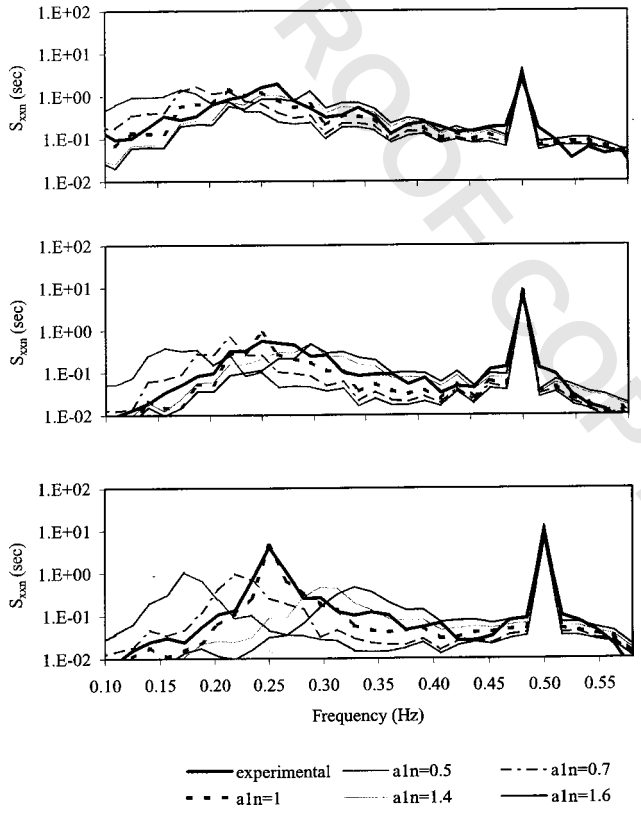

Fig. 6 Effect of a_1 on SDOF system behavior: *a*) (top) SL, *b*) (middle) SM, *c*) (bottom) SH

nonlinear behavior of the complex damping mechanism of the SDOF configuration. In the physical system, with the rod passing through the center of the sphere (to restrict vertical and rotational motions), the Coulomb frictional component is proportional to the magnitude of the normal reaction force between the sphere and the supporting rod. Because the sphere is neutrally buoyant, this normal force is proportional to the magnitude of the oscillatory lift force. The nonlinear effects become more severe at the lower wave amplitudes prominent due to the sticky (stop and go, highly nonlinear) motion of the sphere, thus affecting the response prediction capability of the model.

Effects of Hydrodynamic Coefficients on System Response

The IFF model requires the knowledge of C_d and C_m for the evaluation of hydrodynamic force on the sphere. As mentioned earlier, the effect of C_m and C_d on the nonlinear response has not been studied before according to the authors' knowledge. In order to investigate the response behavior of the system, C_m is varied within the range of 1–1.5 and the NSND algorithm is then applied. The identified properties are tabulated for different C_m in Table 4. From the table, magnitudes of C_a, a_1, a_2, a_3, C'_d, ζ_s and C_s increase with increasing C_m. The natural frequency identified is constant for all the cases. The responses simulated using the parameters are compared with the measured response in Fig. 11*a*. The primary resonance energy of all the predicted responses is practically constant and agrees favorably with that of the measured response. Note that the subharmonic energy of the predicted

Table 4 Identified system parameters using IFF model by varying hydrodynamic coefficients: C_m and C_d

C_m	C_a	C_d	a_1 N/m	a_2 N/m^2	a_3 N/m^3	C'_d	ζ_s	f_n
1.10	0.11	1.00	119.1	167.4	911.3	0.18	0.021	0.237
1.20	0.21	1.00	122.4	180.3	924.1	0.18	0.033	0.237
1.30	0.32	1.00	132.0	215.7	1020.7	0.18	0.032	0.237
1.40	0.42	1.00	151.3	235.1	1175.3	0.19	0.033	0.237
1.50	0.51	1.00	161.0	244.7	1284.8	0.19	0.035	0.237
C_d	C_m	C_a	a_1 N/m	a_2 N/m^2	a_3 N/m^3	C'_d	ζ_s	f_n
0.20	1.30	0.30	128.8	215.7	972.4	0.18	0.021	0.237
0.50	1.30	0.30	128.8	219.0	988.6	0.18	0.033	0.237
0.80	1.30	0.30	132.0	219.0	1004.7	0.19	0.032	0.237
1.00	1.30	0.30	132.0	219.0	1004.7	0.19	0.035	0.237
1.20	1.30	0.30	132.0	222.2	1020.7	0.19	0.035	0.237

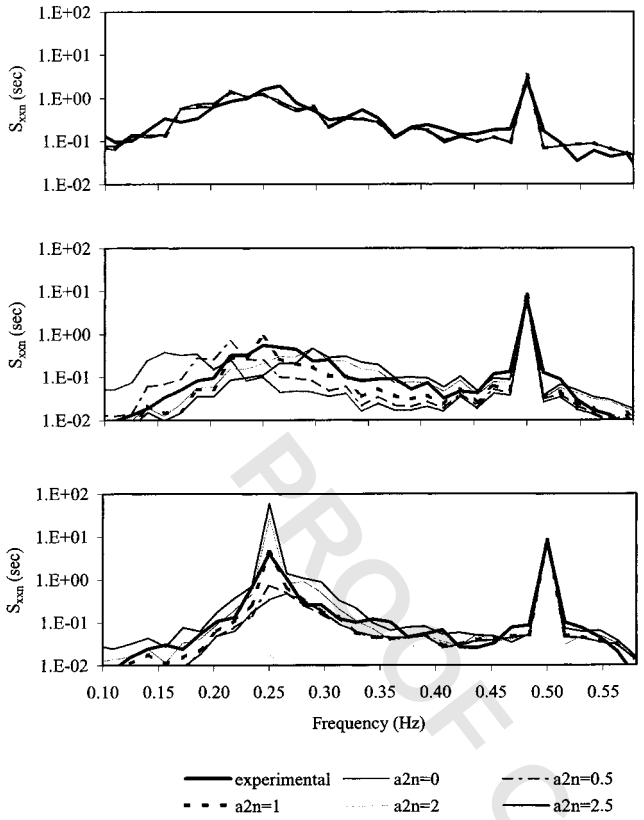

Fig. 7 Effect of a_2 on SDOF system behavior: *a*) (top) SL, *b*) (middle) SM, *c*) (bottom) SH

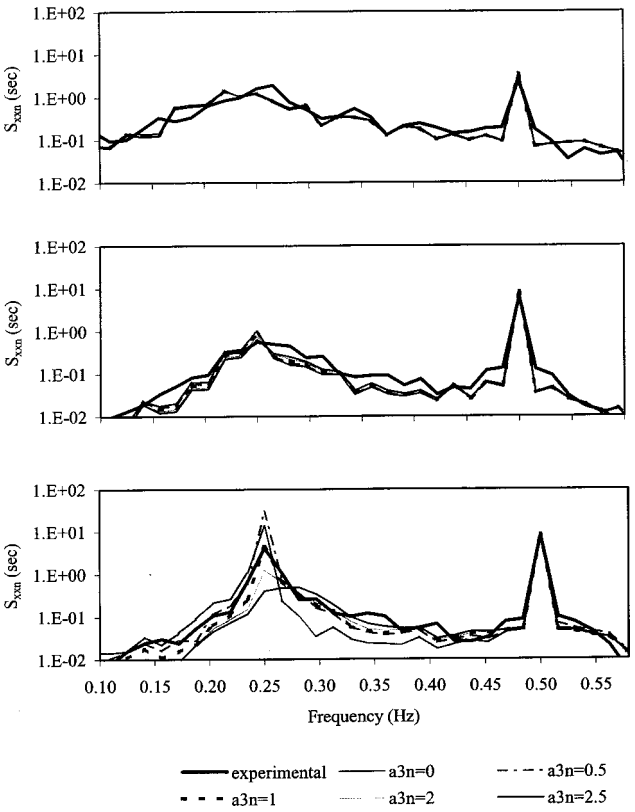

Fig. 8 Effect of a_3 on SDOF system behavior: *a*) (top) SL, *b*) (middle) SM, *c*) (bottom) SH

response decreases with increasing values of inertia coefficient and $C_m = 1.3$ matches well with the experimental response.

The drag coefficient C_d is varied between 0.2—1.0 and the properties are identified in Table 4. The parameters remain consistent for different values of C_d. The responses simulated using the parameters are compared with the measured response in Fig. 11*b*, and it can be observed that the response does not change significantly with varying values of C_d. Based on the water depth to wavelength (h/L) and diameter to wave height (D/H) ratios (Nath and Harleman, 1970), the inertia effects dominate the total forces and the response, as expected, is found to be relatively insensitive to changes in C_d.

Effects of KC and Re on Hydrodynamic Coefficients

It can be observed from the Keulegan-Carpenter number (KC_F for far field in this case), the Reynolds number (Re_F for far field in this case), the inertia coefficient C_m and the drag coefficient C_d for the SDOF experimental data tabulated in Table 1 that the inertia coefficient C_m decreases with increases in KC_F and Re_F. It is observed that C_m varies between 1.1–1.4 for $5.7\times10^4 \leq Re_F \leq 2.3\times10^5$ and $0.56 \leq KC_F \leq 2.2$. Since the inertia effects dominate the total forces for this experiment as explained in the previous section, the response is relatively insensitive to changes in C_d. As shown in Table 1, C_d ranges between 0.1–0.9 for each data set with simulated response matching with that of experimental data.

Conclusion

The applicability of two different models, (A) relative-velocity (RV) and (B) independent flow field (IFF) models and their corresponding algorithms—(A.1) nonlinear-structure linearly damped (NSLD), and (A.2) nonlinear-structure coupled hydrodynamically damped (NSCHD), for the RV model, and (B.1) nonlinear-

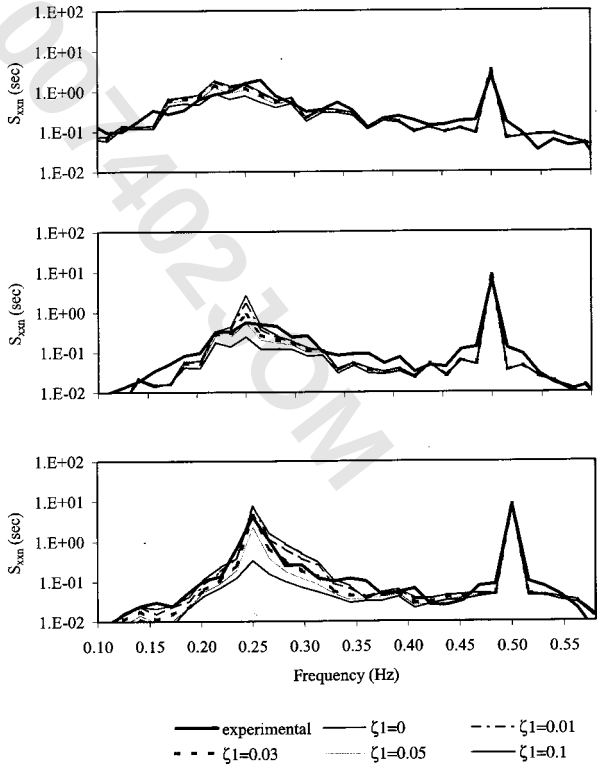

Fig. 9 Effect of ζ_1 on SDOF system behavior: *a*) (top) SL, *b*) (middle) SM, *c*) (bottom) SH

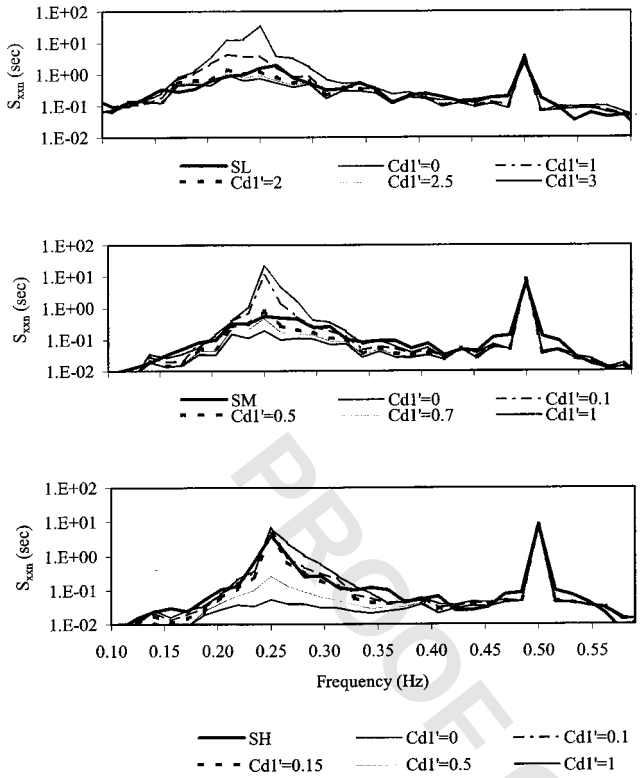

Fig. 10 Effect of C'_{d1} on SDOF system behavior: *a*) (top) SL, *b*) (middle) SM, *c*) (bottom) SH

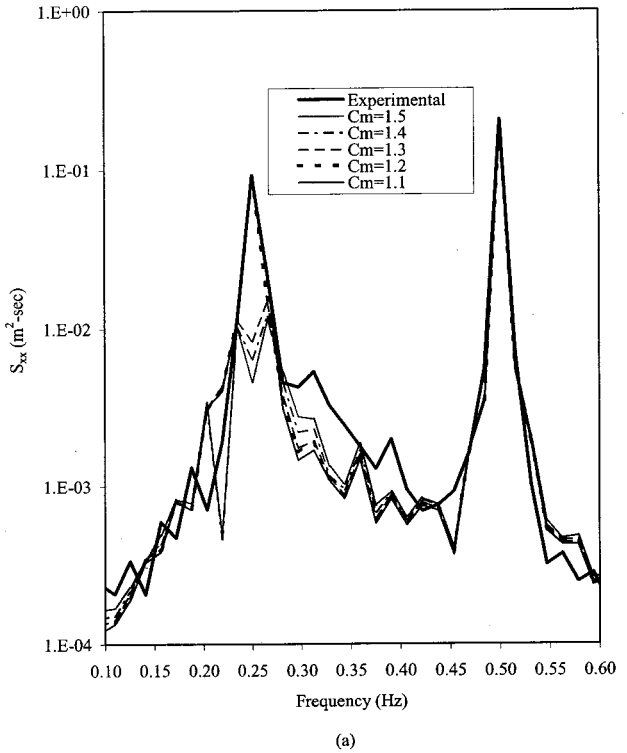

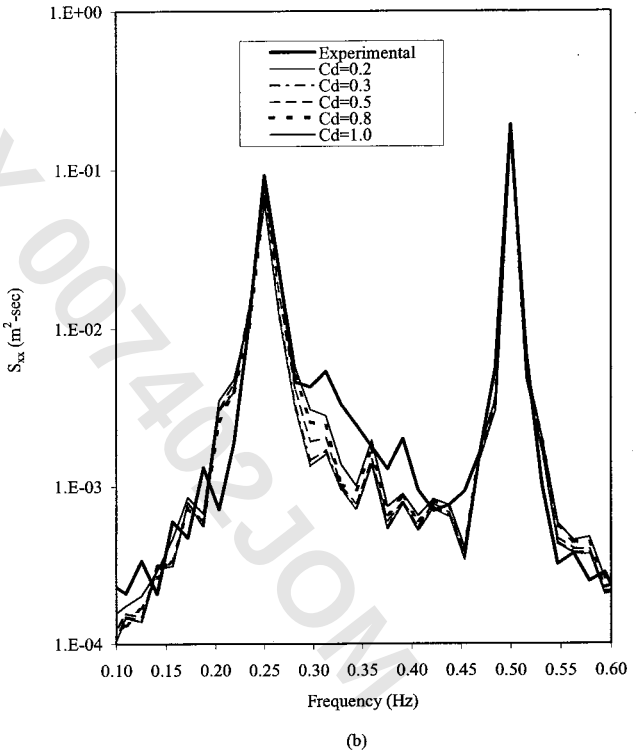

Fig. 11 Comparison of identified response using NSND model with the measured response by varying hydrodynamic coefficients: *a*) C_m, *b*) C_d

structure nonlinearly damped (NSND) for the IFF model developed in Part 1, have been examined. The IFF model with the NSND algorithm is determined to be the most suitable analytical model for the experimental system. The RV models incorporate relative motion hydrodynamic damping and the system properties identified do not predict a comparable response with the measured response. With low Keulegan-Carpenter number and high reduced velocity, the IFF model is found to be more appropriate for the experimental system. The sensitivity analysis of the SDOF system presented here reveals that the effects of variations in system parameters on the predicted responses become more significant with increasing wave excitation amplitude. Three groups are established among the tests depending on low, medium or high wave excitation amplitude based on the response behavior. The response variation becomes more significant with increasing wave amplitude. The optimal value and range of nonlinear structural damping coefficient varies among the tests. This apparent behavior is probably caused by the inability of the model to approximate accurately the actual nonlinear behavior of the complex damping mechanism of the SDOF configuration as the Coulomb frictional component is not included in the mathematical model. The nonlinear effects appear to become more prominent at the lower wave amplitudes, resulting in high values with the errors lumped in the coefficient, C'_{d1}. For the set of experimental data considered, C_m varies between 1.1–1.3 for $5.3\times10^5 \leqslant Re_F \leqslant 7\times10^5$ and $4.7 \leqslant KC_F \leqslant 6.2$ and 1.3–1.5 for $1.3\times10^5 \leqslant Re_F \leqslant 3.7\times10^5$ and $1.2 \leqslant KC_F \leqslant 3.3$. In general, C_m increases with decreasing Reynolds number and Carpenter-Carpenter number. Because the experimental wave-structure interaction characteristics fall within the inertia regime, it is not possible to accurately evaluate the drag coefficients. Indeed, the response is observed to be insensitive to variations in C_d.

Acknowledgment

Financial support from the US Office of Naval Research, Grant No. N00014-92-J-1221, is gratefully acknowledged.

Nomenclature

The following symbols appeared in either Part 1 or Part 2 of these papers.

a = dominant wave amplitude
a_1, a_2 and a_3 = restoring force coefficients
d = distance of the center of the sphere from the wall
$f(t)$ = hydrodynamic force acting on the sphere
$f_a(t)$ = input force
$f_e(t)$ = effective force
f_n = resonance frequency of linearized system
h = water depth
k = wave number
l_c = initial spring length
l_1 and l_2 = spring lengths
m = mass of structure (sphere)
s = distance of the instantaneous center of the sphere from the bottom
u = fluid particle velocity in surge direction
$\dot{u}(t)$ = fluid particle acceleration in surge direction
u_o = amplitude of the water particle velocity
v_{ro} = amplitude of v_r
v_r, = relative velocity
$x(t), \dot{x}(t), \ddot{x}(t)$ = displacement, velocity and acceleration of structure as a function of time t
$\dot{x}_o$ = amplitude of the structure velocity
$A_1(f)$, $A_2(f)$ and $A_3(f)$ = Fourier transform of a_1, a_2 and a_3, respectively
C_a = added mass coefficient
C_d = hydrodynamic drag coefficient
C'_{d1} = linear structural damping coefficient
C'_d = nonlinear structural damping coefficient
C_m = hydrodynamic inertia coefficient
C_s = linear structural damping coefficient (dimensional)
D = diameter of sphere
H = high amplitude
$H(f)$ = frequency response function of an ideal constant parameter linear system
IFF = independent flow field
K = spring constant
KC = Keulegan-Carpenter number
L = low amplitude
M = medium amplitude
NSCHD = nonlinear structure coupled hydrodynamically damped
NSLD = nonlinear-structure linearly damped
NSND = nonlinear-structure nonlinearly damped
R-MI/SO = reverse multiple-input/single output
$R(x(t))$ = restoring force as a function of displacement of the structure
Re = Reynolds number
$R'(x(t))$ = approximate restoring force $R(x(t))$
RV = relative velocity
S = single degree of freedom
T = wave period
T_r = combined period of v_r
T_o = period of oscillation of structure
V_R = reduced velocity
$V(x(t))$ = potential function of displacement x(t)
$X_1(f)$, $X_2(f)$, $X_3(f)$ = Fourier transform of x_1, x_2 and x_3, respectively
$\eta(t)$ = wave elevation
$\xi(t)$ = zero-mean delta-correlated white noise
ζ_1 = linear damping ratio
ν = viscosity of the fluid
ρ = mass density
ω = angular velocity

References

[1] Narayanan, S., and Yim, S. C. S., 2003, "Modeling and Identification of a Nonlinear SDOF Moored Structure, Part 1–Hydrodynamic Models and Algorithms," ASME J. Offshore Mech. Arct. Eng., *(submitted for publication)*.
[2] Yim, S. C. S., Myrum, M. A., Gottlieb, O., Lin, H., and Shih, I-M., 1993, *Summary and Preliminary Analysis of Nonlinear Oscillations in a Submerged Mooring System Experiment*, Oregon State University, Ocean Engineering Report No. OE-93-03.
[3] Wang, C. Y., 1965, "The Flow Induced by an Oscillating sphere." J. Sound Vib., **2**(3), pp. 257–267.
[4] Hjelmfelt, A. T., Carney, III, J. F., Lee, S. L., and Mockros, L. F., 1967, "Dynamic Response of a Restrained Sphere in a Fluid," J. Eng. Mech. Div., **93**, pp. 41–56.
[5] Harleman, D. R. F., and Shapiro, W. C., 1958, "Investigations on the Dynamics of Moored Structures in Waves," M. I. T. Hydrodynamics Lab. Tech. Rept. No. 28. Hjelmfelt, A. T., et al., 1967, "Dynamic Response of a Restrained Sphere in a Fluid," J. Eng. Mech. Div., **93**, pp. 41–56.
[6] Grace, R. A., and Zee, G. T. Y., 1978, "Further Tests on Ocean Wave Forces on Sphere," J. Waterway Port Coastal and Ocean Div., **104**, pp. 83–88.
[7] Grace, R. A., and Casiano, F. M., 1969, "Ocean Wave Forces on a Sub Surface Sphere," J. Waterways and Harbor Div., **95**, pp. 291–312.
[8] Gerald, G. F., and Wheatley, P. O., 1989. *Applied Numerical Analysis*, Addison-Wesley Publishing Company.
[9] Laya, E. J., Connor, J. J., and Shyam Sundar, S., 1984, "Hydrodynamic Forces on Flexible Offshore Structures," J. Eng. Mech. Div., **123**, pp. 433–488.